Journal of Zhejiang University-SCIENCE A (Applied Physics & Engineering)
ISSN 1673-565X (Print); ISSN 1862-1775 (Online)
www.jzus.zju.edu.cn; www.springerlink.com
E-mail: jzus@zju.edu.cn

Characteristics of mixing enhancement achieved using a pulsed plasma synthetic jet in a supersonic flow*

Peng WANG, Chi-bing SHEN†‡

Science and Technology on Scramjet Laboratory, College of Aerospace Science and Engineering, National University of Defense Technology, Changsha 410073, China

†E-mail: cbshen@nudt.edu.cn

Received Mar. 29, 2019; Revision accepted Aug. 16, 2019; Crosschecked Aug. 22, 2019

Abstract: Supersonic mixing layers exist extensively in supersonic engineering applications. The rapid mixing of fuel and oxidant at short distances is of great importance, but makes it difficult to develop efficient propulsion systems. The plasma synthetic jet (PSJ) is regarded as a promising high-speed flow control technique. The characteristics of mixing enhancement achieved using a pulsed PSJ were investigated via experiments. Results showed that the PSJ is an effective method for mixing enhancement. Nanoparticle-based planar laser scattering (NPLS) was used to obtain flow structures in three directions. The velocity fields near the PSJ actuator orifice were measured by particle image velocimetry (PIV). Indexes of the fractal dimension and mixing layer thickness were applied to estimate the effect of the PSJ actuator on the supersonic mixing layers. The large-scale vortex structures induced by the pulsed PSJ in the supersonic mixing layers were successfully captured by NPLS. The effect of the PSJ on the supersonic mixing layers was remarkable. The mixing layer thickness under perturbation was larger than that under no perturbation in the downstream. The distribution of the fractal dimension suggests that perturbation of the PSJ cannot improve the fractal dimension values of the fully developed supersonic mixing layers.

Key words: Supersonic shear layers; Supersonic mixing layers; Plasma synthetic jet (PSJ); Mixing enhancement
https://doi.org/10.1631/jzus.A1900130 **CLC number:** V23; V43

1 Introduction

Supersonic mixing layers are found extensively in supersonic aircraft, such as in scramjet combustors, nozzle exits, and cavities on the outer surfaces of air vehicles. In a scramjet engine, the rapid and efficient mixing of fuel and oxidant can reduce the length of the combustor and improve combustion efficiency (Gutmark et al., 1995; Zang et al., 2005; Anderson and Knight, 2012; Zhang et al., 2018). The combustion residence time does not exceed milliseconds due to the high speed of the two streams (Haimovitch et al., 1994). Knowing how to achieve the rapid and efficient mixing of fuel and oxidant is one of the key requirements for scramjets (Liao et al., 2018). The exhaust jet is the source of noise and infrared signals. Its noise must be reduced for environmental reasons (McCormick and Bennett Jr, 1994; Dietiker and Hoffmann, 2007). Moreover, dissipating the heat signature can improve stealthiness for military purposes (Martens and McLaughlin, 1995; Lui and Lele, 2001; Collin et al., 2004). Noise and infrared signals can be reduced by increasing the mixing between the jet and the ambient flow. Internal cavities used for carrying weapons are frequently found in supersonic air vehicles (Lazar et al., 2008). The mixing layers must be enhanced to successfully release weapons.

The growth rate of supersonic mixing layers is slower than that of their subsonic counterparts (Guirguis et al., 1987). Compressibility considerably

‡ Corresponding author
* Project supported by the National Natural Science Foundation of China (No. 11572346)
ORCID: Peng WANG, https://orcid.org/0000-0002-8833-6056

reduces the mixing layer growth rate in supersonic flows. Seeking an effective mixing enhancement method is important in supersonic flows. Mixing enhancement methods can be divided into two general categories: passive and active methods (Seiner et al., 2001; Watanabe and Mungal, 2005). Passive methods involve geometrically modifying the trailing edge structure to realize mixing enhancement (Fernando and Menon, 1993; Kharitonov et al., 2000). Common passive mixing enhancement configurations are lobes, saw teeth, and other special shapes on trailing edge structures. Although these configurations are simple and easy to use, passive mixing enhancement methods cannot be varied as conditions change (Collin et al., 2004). In active mixing enhancement methods, energy is periodically injected into the flow field (Adelgren et al., 2005; Freeman and Catrakis, 2009). Common active mixing enhancement methods include mechanical vibration (Zhang et al., 2015), synthetic jets (Davis and Glezer, 1999; Tamburello and Amitay, 2008), and discharge excitation (Benard et al., 2008). Active mixing enhancement methods have more advantages than passive methods, and can improve mixing with a lower total pressure loss. Although traditional active mixing enhancement methods are relatively effective, they still have some deficiencies, such as a low energy density, high gas supply requirement, and low working frequency.

A plasma synthetic jet (PSJ) is an effective flow control method which can avoid the aforementioned deficiencies. A PSJ is appealing for flow control due to its high energy density and rapid response (Narayanaswamy et al., 2008). Moreover, a PSJ does not require additional gas supply and mechanical parts. A PSJ actuator, also called a spark jet or pulsed plasma jet, was developed in 2003 by the Applied Physics Laboratory at Johns Hopkins University, USA (Grossman et al., 2003, 2004). A PSJ works by striking a short duration high-current electric arc in a closed cavity with an exit orifice. The plasma generated by the arc discharge does not come into direct contact with the controlled flow field. The temperature and pressure of the gas inside the cavity increase rapidly due to electrothermal heating. High-pressure gas bursts forth through the orifice and controls the flow field.

Turbulent mixing can be viewed as a three-stage process of entrainment, dispersion (or stirring), and diffusion, which together span the full space-time scale spectrum of a flow (Dimotakis, 1991). To achieve mixing enhancement, the entrainment must first be enhanced. A PSJ is used to induce a large-scale vortex and realize the mixing enhancement.

Hardy et al. (2010) used a PSJ to enhance mixing in a subsonic shear layer. Their results showed that the large-scale vortex structure induced by a PSJ can increase the thickness of the mixing layer. Huet (2014) numerically investigated the control and noise reduction of a subsonic jet with a PSJ. Chedevergne et al. (2015) investigated the response of an isothermal jet with a high Reynolds number (Ma=0.6) to a PSJ actuator via phase-locked particle image velocimetry measurements and numerical simulations. Narayanaswamy et al. (2012) studied the control of supersonic flow using a PSJ.

There have been few studies of the use of PSJs to enhance the mixing of supersonic layers. Wang and Shen (2019) were first to use a PSJ to enhance the mixing of supersonic layers. Their numerical simulation results indicate that the position of the actuators can influence the mixing enhancement effect. The remarkable perturbations of the PSJ on the supersonic mixing layers were proved by experimental results.

The objective of the present study was to investigate experimentally the characteristics of mixing enhancement achieved using a pulsed PSJ in a supersonic flow. The velocity fields near the PSJ actuator orifice were measured by particle image velocimetry (PIV). The instantaneous flow structures of the supersonic mixing layers in three directions were captured by nanoparticle-based planar laser scattering (NPLS). The evolution of the large-scale vortex structures induced by the PSJ was also investigated. Indexes of the fractal dimension and mixing layer thickness were used to analyze the characteristics of the mixing enhancement.

2 Actuator description and experimental setup

The experiments were conducted in the low-noise supersonic mixing layers of the wind tunnel described by Wang et al. (2013), Feng et al. (2015), and Wang and Shen (2019) (Fig. 1). Air, as the inflow, flowed into the wind tunnel due to a pressure difference between the environment and the vacuum tank. The test section was 350 mm long and 200 mm wide.

To eliminate the streamwise pressure gradient, the upper and lower walls were diverged by 1°. The test section was symmetrical and nearly horizontal. A 10-mm thick flat splitter was embedded along the centerline from the inlet of the wind tunnel to the outlet of the Laval nozzle, thereby separating the wind tunnel into two halves to obtain two different Mach numbers at the outlet of the nozzle. The total pressure controller of the upper stream was used to realize a static pressure match in the test section. The flow field was calibrated in the experiment. The calibrated convective Mach number (*Mc*) in the experiment was 0.30, with Mach numbers of 2.39 for the lower stream and 1.37 for the upper stream. The convective Mach number can be calculated by (Bogdanoff, 1983; Papamoschou, 1989)

$$Mc = \frac{U_1 - U_2}{a_1 - a_2}, \tag{1}$$

where U_1 is the upper stream velocity, U_2 is the lower stream velocity, a_1 is the upper stream sonic velocity, and a_2 is the lower stream sonic velocity. The flow parameters are shown in Table 1.

The detailed mechanisms of the PSJ have been reported in (Santhanakrishnan and Jacob, 2007; Haack et al., 2011; Wang et al., 2014b; Zhou et al., 2017). A schematic of the PSJ actuator location is presented in Fig. 2, which also shows the Cartesian coordinate system. *X*, *Y*, and *Z* denote the streamwise, transverse, and spanwise directions, respectively. The PSJ actuator installed in the splitter plate 15 mm upstream of the splitter plate end was used to perturb flow. The actuator consisted of a cylindrical cavity and a pair of tungsten electrodes each of 1-mm diameter. The anode-to-cathode electrode spacing was 1 mm. The cylindrical cavity, composed of resin, had a diameter of 12 mm and a length of 6 mm. The cavity also had a jet hole with a diameter of 2.5 mm (Fig. 3) (Wang and Shen, 2019). A high-voltage pulse power supply was used to excite the actuator. The output voltage could reach 10 kV with an adjustable repetition frequency of 0–100 Hz, and the discharge current could exceed 250 A. The maximum output energy of

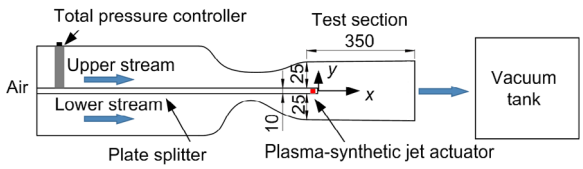

Fig. 1 Schematic of the supersonic wind tunnel (unit: mm). Reprinted from (Wang and Shen, 2019), Copyrights 2019, with permission from *Acta Physica Sinica*

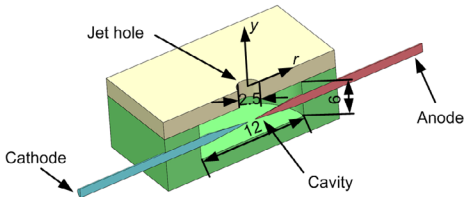

Fig. 3 Two-electrode plasma synthetic actuator (unit: mm). Reprinted from (Wang and Shen, 2019), Copyrights 2019, with permission from *Acta Physica Sinica*

Table 1 Flow parameters of the supersonic mixing layer

Stream	Inflow Mach number, Ma_1, Ma_2	Convection Mach number, Mc	Velocity, U_1, U_2 (m/s)	Total pressure, P_{o1}, P_{o2} (kPa)	Static pressure, P_{s1}, P_{s2} (kPa)	Static temperature, T_{s1}, T_{s2} (K)	Total temperature, T_{o1}, T_{o2} (K)
Upper	1.37	0.3	405.16	21.5	7.0	218.39	300.00
Lower	2.39	0.3	567.18	101.0	7.0	139.87	300.00

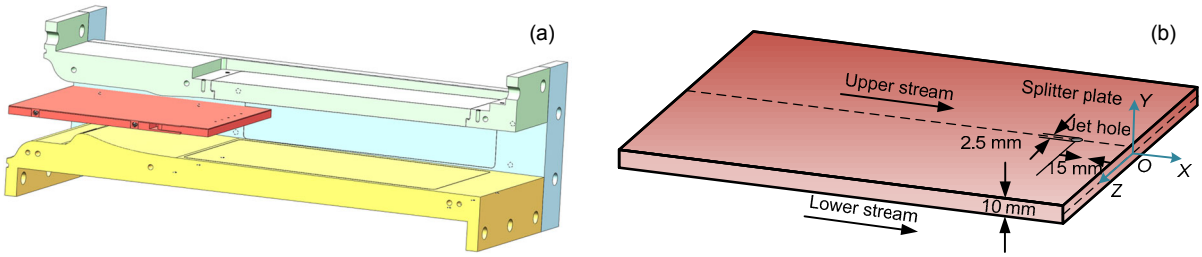

Fig. 2 Schematic of the wind tunnel (a) and the actuator mounted (b) inside a plate

Fig. 2a is reprinted from (Wang and Shen, 2019), Copyrights 2019, with permission from *Acta Physica Sinica*

one pulse was 20 J (Wang et al., 2014a). An energy–storage capacitor of 640 nF was used. The breakdown voltage was about 4.12 kV. The anode–cathode voltage was measured by a high-voltage probe (Tektronics P6015A, USA). The voltage was recorded using an oscilloscope (Tektronix DPO3014, USA). The real energy E of the capacitor was determined by

$$E=\frac{1}{2}CU_{\text{voltage}}^2, \tag{2}$$

where C is the capacity, and U_{Voltage} is the voltage. The capacitive energy was about 5.43 J.

The NPLS experimental system developed by Zhao (2008) based on Rayleigh scattering was used in the experiments to obtain instantaneous images of the flow field. The system consisted of a double-pulsed Nd:YAG laser with a wavelength of 532 nm and a pulse energy of 350 mJ per 6 ns, a charge-coupled device (CCD) camera with 4008 pixels×2672 pixels, a synchronizer for the pulsed laser and the CCD camera, a nanoparticle generator, and a computer. TiO_2, which has an effective diameter of 42.5 nm and a relaxation time of 66.3 ns, was selected as the tracer nanoparticles based on the work of Zhao (2008). The high strength of TiO_2 is attributed to the fluctuation of the small-scale turbulence of the supersonic flow. The gray level of the flow field images is proportional to the concentration of nanoparticles in the imaging planes. The concentration of nanoparticles is dependent on the density field. Thus, the gray level of the flow field images can reflect the density field. The NPLS system was used to capture the high-resolution characteristics of the flow field in the streamwise, spanwise, and transverse planes. The spanwise (X-Y) plane is located at the middle part of the actuator's orifice. The area denoting these NPLS instantaneous results is 150 mm×60 mm. The instantaneous results in the streamwise plane (Y-Z) located at x=60 mm, and the transverse (X-Z) plane located at y=0 mm, were also obtained.

The same equipment was used for PIV and NPLS. The time interval between two frames of a PIV image pair was set at 500 ns. PIV was used to obtain the velocity fields near the actuator orifice.

The NPLS/PIV frequency of the operation was only 2 Hz, and the exposure time of the camera was only 6 ns. The influence time of the single-pulsed PSJ on the supersonic shear layer was considerably less than 1 ms. The traveling of the perturbations introduced by the pulsed PSJ to the appropriate location for observation also required spending time. In experiments under these conditions, the NPLS system began to operate when the PSJ began to operate after a delay time. The PSJ electronic system and the NPLS system were controlled by a signal source. This command was applied to trigger NPLS with a controllable delay (Δt). Fig. 4 is a schematic of the experimental system control sequence chart (Wang and Shen, 2019).

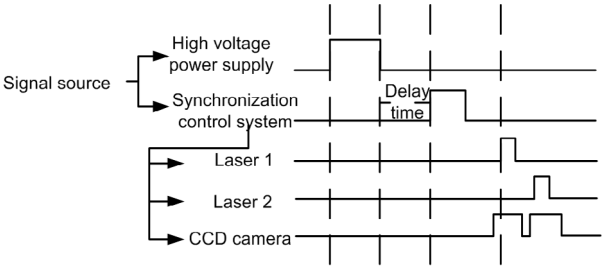

Fig. 4 Schematic of the experimental system sequence chart. Reprinted from (Wang and Shen, 2019), Copyrights 2019, with permission from *Acta Physica Sinica*

3 Results and discussion

3.1 Velocity fields near the PSJ actuator orifice

Fig. 5 is a schematic of the experimental arrangement for obtaining the velocity fields in the X-Y plane. D denotes the diameter of jet hole. The position of the sheet optics was at z=0 mm. T_0 is defined as the moment that the discharge began. Fig. 6 shows the T_0+20 μs PIV results, and Fig. 7 shows the T_0+110 μs PIV results. U denotes the X-velocity, and V denotes the Y-velocity. At T_0+20 μs, the upper stream was lifted by the PSJ. At T_0+110 μs, a bow shock wave was produced by the PSJ. The upper stream was deflected upwards and its velocity decreased behind the bow shock wave. The velocity of the upper stream, U_∞=350 m/s, was measured by PIV. The transverse velocity near the PSJ actuator orifice was regarded as the jet speed V_{jet}. At T_0+20 μs, the jet speed was about 174 m/s, and the speed ratio between the jet and the upstream flow was V_{jet}/U_∞=0.497. At T_0+110 μs, the

jet speed was about 180 m/s, and the speed ratio between the jet and the upstream flow was V_{jet}/U_{∞}= 0.514.

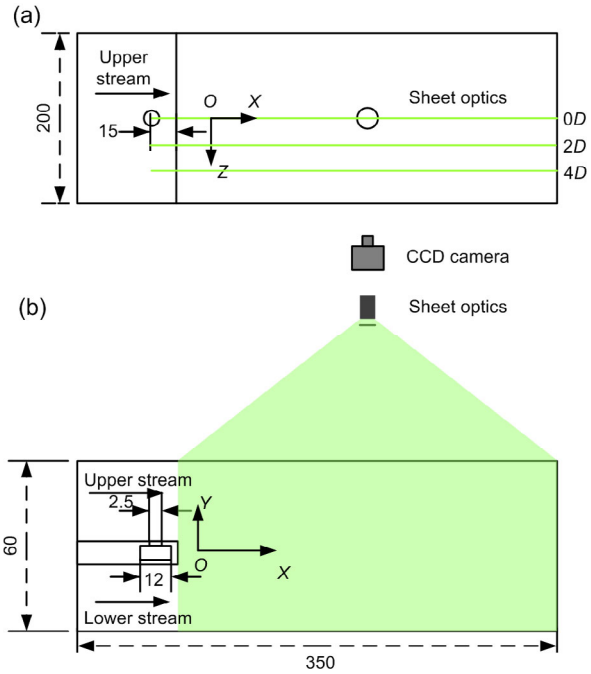

Fig. 5 Schematic of the experimental arrangement for obtaining the flow characteristics in the *X*-*Y* plane: (a) top view; (b) side view (unit: mm)

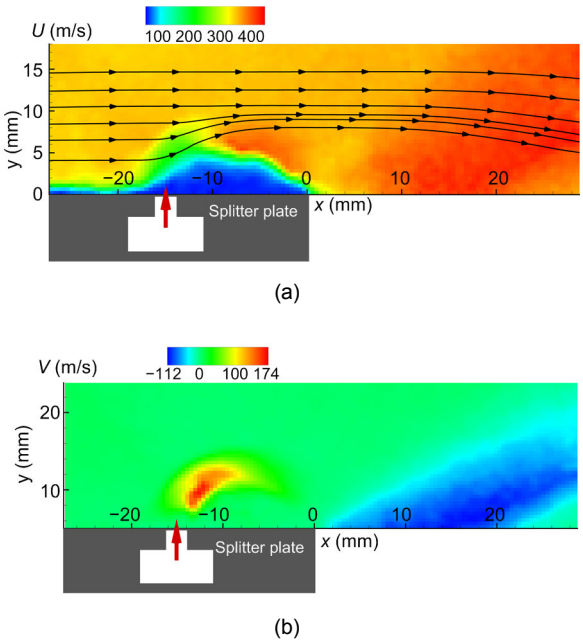

Fig. 6 T_0+20 μs PIV results: (a) *U* (m/s); (b) *V* (m/s)

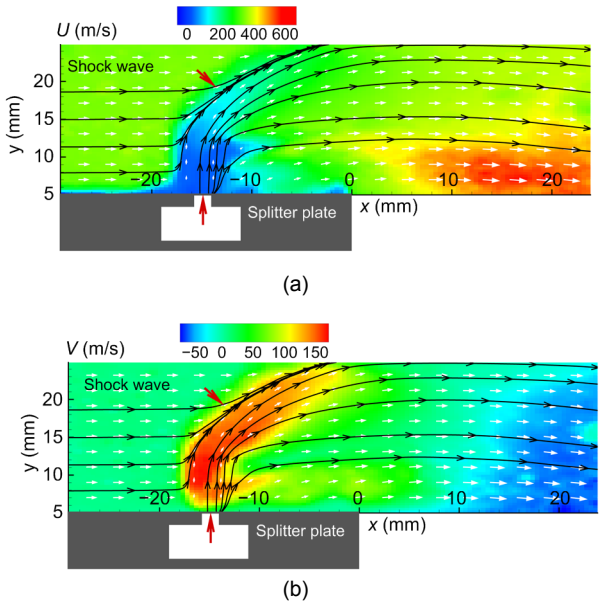

Fig. 7 T_0+110 μs PIV results: (a) *U* (m/s); (b) *V* (m/s)

3.2 Effect of the PSJ on supersonic mixing layer development in the *X*-*Y* plane

A schematic of the experimental arrangement is shown in Fig. 5. The two streams met and produced a reattachment shock wave at the reattachment point (Fig. 8a). The redevelopment of the mixing layer was generated, and the vortex rolled up after the reattachment point. A recirculation zone was present at the edge of the splitter plate. The mixing layer was inclined to the upper (low-speed) stream (Fig. 8a), which can be attributed to the entrainment of a volume of the fluid from the two freestreams into the turbulent mixing layer that was not symmetric. The volume of the entrainment fluid from the low-speed freestream was greater than that from the high-speed freestream. The deflection of the mixing layer intensified behind an oblique shock wave which passed through it at about x=65 mm.

Inside the chamber, an arc discharge was struck and the air was heated and pressurized. Hot pressurized air spurted out due to air expansion. The air became a jet with a high temperature and low density, which interacted with the supersonic mixing layer. The effect of PSJ excitation on the supersonic shear layer was evidently strong (Fig. 8b). The large-scale vortex structures induced by the PSJ can be easily distinguished. The Kelvin-Helmholtz instability was intensified, and the Kelvin-Helmholtz vortices under

perturbation were larger than those under no perturbation. A black ribbon structure was lacking in the two freestreams (Fig. 8b). The structure was presumed to be the jet produced by the PSJ actuator.

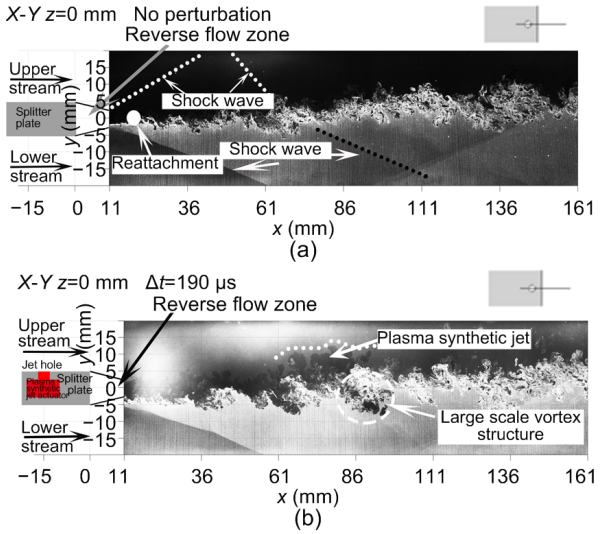

Fig. 8 NPLS images of the supersonic mixing layer under no perturbation (a) and perturbation (b)

3.3 Effect of the PSJ on supersonic mixing layer development in the *X-Z* plane

Fig. 9 is a schematic of the experimental arrangement for obtaining the velocity flow characteristics in the *X-Z* plane. The intermittent large-scale vortex structures of the PSJ are presented in Fig. 10. The first three vortices are larger than the latter two. The perturbation had not spread downstream. The first three vortices were induced by the PSJ. The generation and development of the latter two vortices were not affected by the PSJ perturbation.

3.4 Effect of the PSJ on supersonic mixing layer development in the *Y-Z* plane

Fig. 11 is a schematic of the experimental arrangement for obtaining the velocity flow characteristics in the *Y-Z* plane. This method causes deformation of images in the *Y* direction. Refraction occurred due to the heavy sheet glass. The method of shooting and the refraction of the glass led to the poor definition. The rough shape of the PSJ in the *Y-Z* plane can be identified from the NPLS results.

The NPLS results for the *Y-Z* plane at the location of x=60 mm are presented in Fig. 12. The PSJ perturbations are obvious in the *Y-Z* plane. The shape of the PSJ was a near-circle. Small-scale vortex structures, which are conducive to mixing enhancement, were present inside the jet.

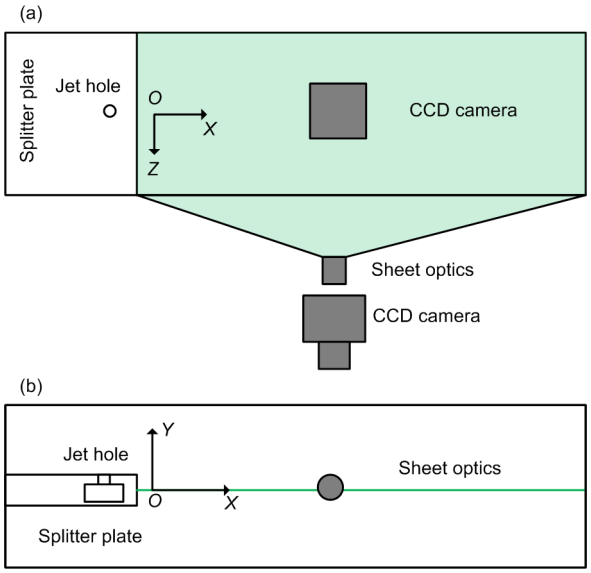

Fig. 9 Schematic of the experimental arrangement for obtaining the flow characters in the *X-Z* plane: (a) top view; (b) side view

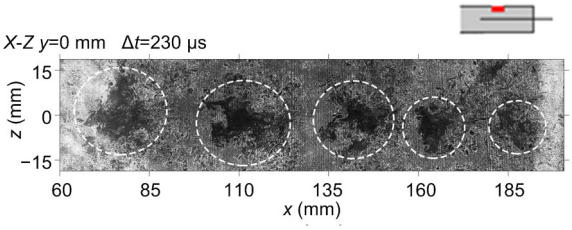

Fig. 10 NPLS image of the supersonic mixing layer with perturbation at *y*=0 mm in the *X-Z* plane

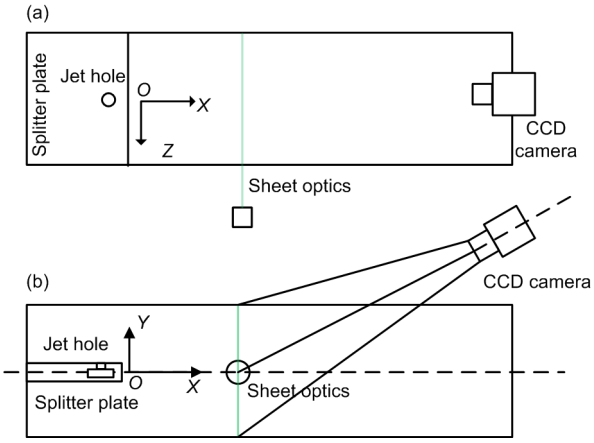

Fig. 11 Schematic of the experimental arrangement for obtaining the flow characters in the *Y-Z* plane: (a) top view; (b) side view

3.5 Effect of the PSJ on supersonic mixing layers in the *X-Y* plane at different spanwise positions

The spanwise plane z was made dimensionless as $Z^*=z/D$. The high resolution structures of the flow field at $Z^*=0$, $Z^*=2$, and $Z^*=4$ were obtained by NPLS. A schematic of the experimental arrangement is provided in Fig. 5.

The NPLS results for different locations in the spanwise plane given the same delay time are presented in Fig. 13. The effect of the PSJ decreased as the distance from the jet hole increased in the spanwise plane. Perturbation was apparent at $Z^*=0$ and $Z^*=2$ for the NPLS results. Although the perturbation at $Z^*=4$ was smaller than that at $Z^*=2$, the vortices in the supersonic mixing layer under perturbation were greater than that under no perturbation. The perturbation of the PSJ was symmetrical about the *X-Y* plane in the spanwise plane. The effect of the PSJ exceeded 8D in the spanwise plane.

3.6 Effect of the PSJ on vortex evolution in the *X-Y* plane at z=0 mm

The two NPLS visualization results with a time interval of 50 μs are presented in Fig. 14. The size of large-scale vortex structure 2 was smaller than that of large-scale vortex structure 2′, as shown by a comparison between the two images. The large-scale vortex structure appeared to be growing larger. We can therefore infer from the experiment that the evolution mechanism of the large-scale vortex structures was distinctive. We assume that the gas expansion produced by the pulsed PSJ actuator was responsible for the growth of the large-scale structures. The

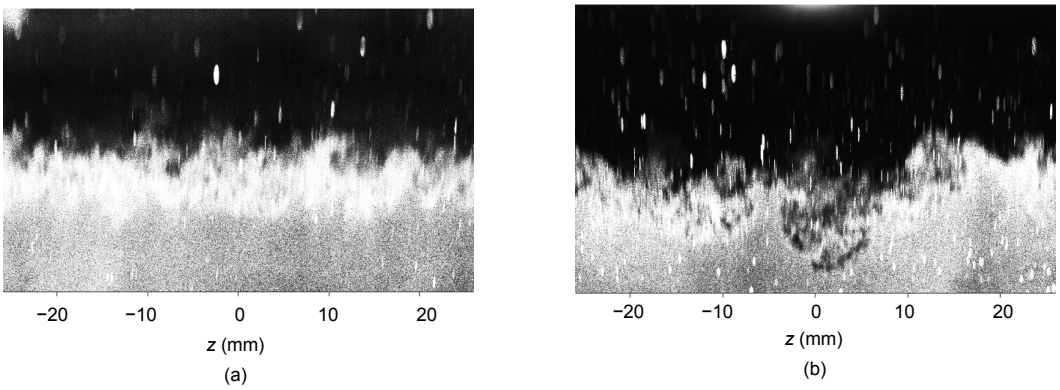

Fig. 12 NPLS results at x=60 mm in *Y-Z* plane: (a) no perturbation; (b) perturbation

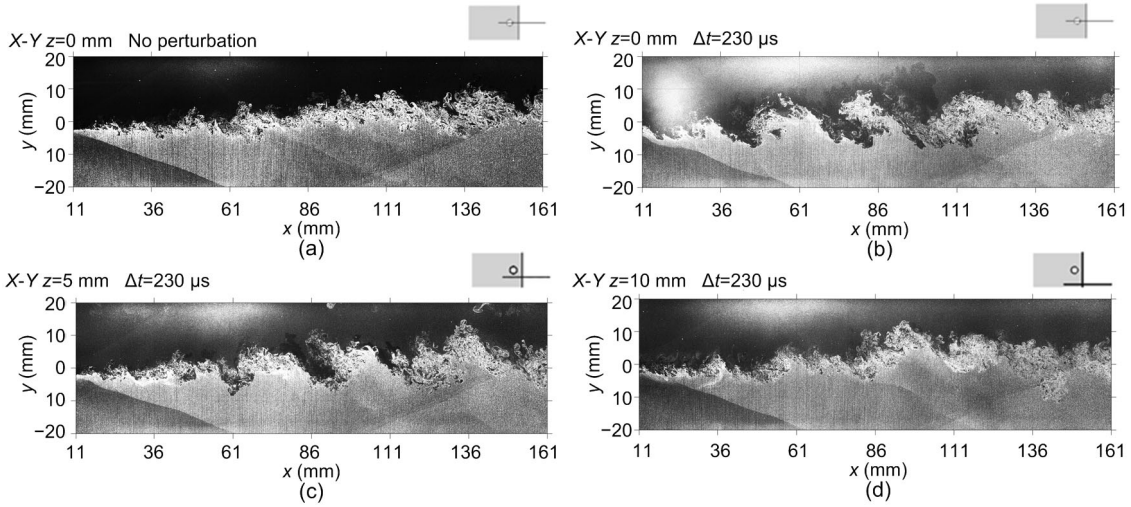

Fig. 13 NPLS image of the supersonic mixing layer with perturbation at different spanwise locations
(a) z=0 mm, no perturbation; (b) z=0 mm, Δt=230 μs; (c) z=5 mm, Δt=230 μs; (d) z=10 mm, Δt=230 μs

structures may shrink as the gas cools. The PSJ inside the large-scale vortex structures intensified the turbulent fluctuation, and the PSJ surrounding the large-scale vortex structures enlarged the vortex scale. The merging trend of the vortices can be explained by the growth of the large-scale vortex structures 1 and 2. The pressure and volume of the PSJ between the two large-scale vortex structures decreased due to temperature reduction, which is advantageous for vortex merging.

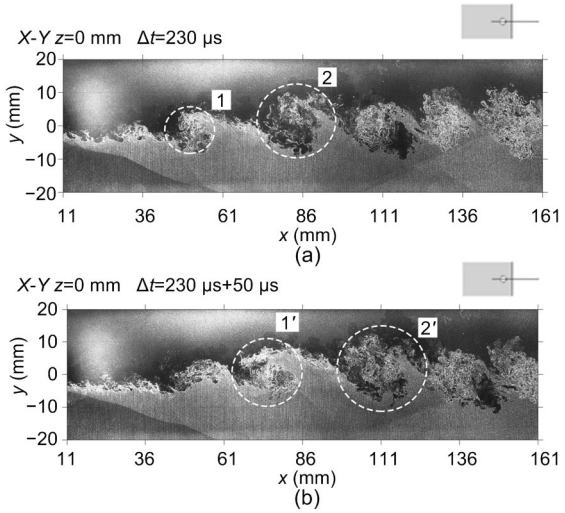

Fig. 14 A pair of instantaneous NPLS visualization results with a time interval of 50 μs
(a) z=0 mm, Δt=230 μs; (b) z=0 mm, Δt=230 μs+50 μs

3.7 Effect of the PSJ on supersonic mixing layers with different delays in the *X-Y* plane at z=0 mm

The flow structures of the supersonic mixing layer with perturbation for different delays are shown in Fig. 15. Note that these images are not temporally relevant. The large-scale vortex structures induced by the PSJ gradually grew and moved downstream of the flow field as the delay Δt increased. Complex small-scale structures appeared inside the large-scale vortex structures induced by the PSJ. These small-scale structures were conducive to well-distributed mixing. The perturbation moved downstream, and the large-scale vortex structures began to break down over time. The large-scale vortex structures in the mixing layer disturbed by the PSJ were larger than those that were undisturbed. This finding indicates that the plasma not only can induce large-scale structures, but also promotes well-distributed mixing. The results show that the perturbation duration of the PSJ can exceed 100 μs.

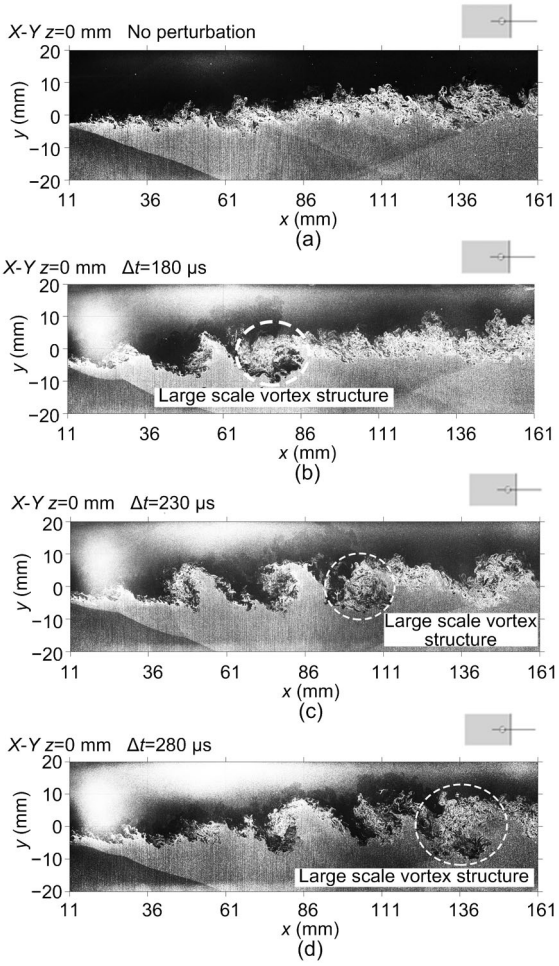

Fig. 15 NPLS image of the supersonic mixing layer with perturbation for different delays
(a) z=0 mm, no perturbation; (b) z=0 mm, Δt=180 μs; (c) z=0 mm, Δt=230 μs; (d) z=0 mm, Δt=280 μs

3.8 Effect of the PSJ on the thickness of supersonic mixing layer for different delays in the *X-Y* plane at z=0 mm

The thickness of the supersonic mixing layer is an important indicator for evaluating the effect of mixing enhancements. To measure the thickness, the turbulent interface of the supersonic mixing layer needs to be extracted from the NPLS results. The local self-adapted threshold value processing method was used to fix the position of the interface, and the Canny method was used to detect the edge of the interface (Gonzalez and Woods, 2010). Fig. 16 illustrates the edge detection images.

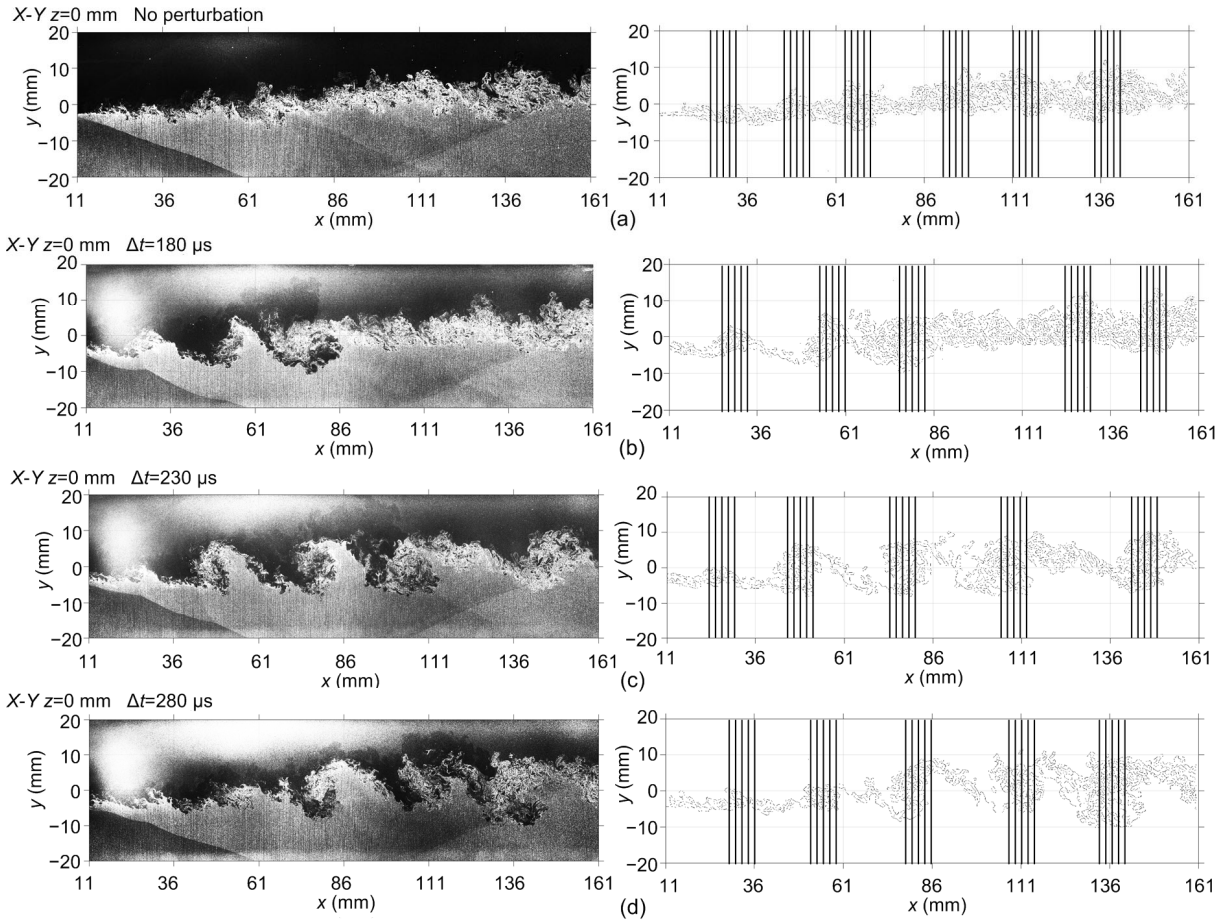

Fig. 16 Edge detection images of flow structures in the supersonic mixing layer for three delays and no perturbation
(a) z=0 mm, no perturbation; (b) z=0 mm, Δt=180 μs; (c) z=0 mm, Δt=230 μs; (d) z=0 mm, Δt=280 μs. Left: NPLS results; right: curves of edge detection

There are many definitions of mixing layer thickness. In this study, a definition was selected according to the experimental data. Hence, the mixing layer thickness denoted by δ was defined as being determined by the size of the large-scale vortex structures (Zhao, 2008). The transverse measurement of the turbulent interface at the location of the vortex was regarded as the thickness of the supersonic mixing layer. There are several sets of vertical lines in Fig. 16. The vertical lines represent the sampling cross sections. The locations of the vertical lines mark the area of the large-scale structures (Fig. 16). A set of vertical lines intersect the turbulent interface. The difference between the maximum and the minimum of the intersections was taken as the average thickness of the supersonic mixing layers. Fig. 17 shows the thickness of the supersonic mixing layer for different delays under perturbation conditions. The thickness under the delay Δt=230 μs condition was thicker than that under the delay Δt=180 μs condition, and the thickness under the delay Δt=180 μs condition was thicker than that under no perturbation. In the delay Δt=280 μs condition, because of the large-scale vortex structures induced downstream by the PSJ convection, the thickness was much greater than that under no perturbation in the downstream. The highest thickness value under the delay Δt=280 μs condition at about x=132 mm was 21 mm, which is 47% higher than that under the no perturbation condition (14.42 mm), given the same position. Notably, with the perturbation of the moving downstream, the effect of the perturbation became relatively large. The PSJ can therefore increase the thickness of the supersonic mixing layer.

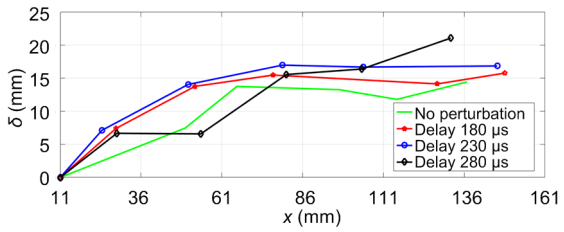

Fig. 17 Variation in the mixing layer thickness under different delays perturbation conditions

3.9 Effect of the PSJ on the supersonic mixing layer fractal dimension for different delays in the *X*-*Y* plane at *z*=0 mm

The fractal dimension is a geometric quantity used to describe the degree of fragmentation of irregular curves (Sreenivasan, 1991). A higher fractal dimension value indicates that the turbulent fluctuation of a flow is more intense, which can greatly contribute to mixing enhancement. Many methods are used to calculate the fractal dimension. The boxing-counting dimension method was used for analysis because it is highly suitable for calculating the dimensions of turbulent and non-turbulent interfaces (Zhao et al., 2008). The boxing-counting dimension method can be briefly described as follows. The mixing layer interface F is covered with area elements of decreasing size, and the numbers of required elements are counted. The size of an element is denoted by $\lambda\times\lambda$, and $N_\lambda(F)$ is used to represent the number of required elements. When the size of the element approaches zero, the negative slope of the fitted line of $\log(N_\lambda(F))$ vs. $\log(\lambda)$ is treated as the dimension. The fractal dimension of the mixing layer interface is defined as (Falconer, 2003)

$$M=\operatorname*{Dim}_{\lambda\to 0}(F)=\frac{\log(N_\lambda(F))}{-\log(\lambda)}. \tag{3}$$

Each NPLS image was divided into six parts, from 11 mm to 161 mm, in the streamwise direction. Each part had a size of 600 pixels×1000 pixels, and the fractal dimension of each part was calculated separately. Fig. 18 shows the distribution of the fractal dimension of the supersonic mixing layer along the streamwise direction for different delay conditions. The values of the fractal dimension under the delay Δt=230 μs condition and no perturbation condition were larger than those of the delay Δt=230 μs and Δt=280 μs conditions from x=61 mm to x=161 mm. According to the NPLS results (Fig. 16), the large-scale vortex structures of delay conditions Δt=230 μs and Δt=280 μs were larger than those of the delay conditions Δt=180 μs and no perturbation. However, the total numbers of small-scale vortex structures were smaller than that for the no perturbation result. The large number of small-scale structures can be observed towards the left of the large-scale vortex structures induced by the PSJ. Towards the right of the large-scale vortex structures, the number of small-scale vortex structures was small. The high-strength perturbation of the PSJ can improve the number of small-scale vortex structures in the local area, but not over the entire mixing layers. In summary, the perturbation of the PSJ cannot improve the value of the fractal dimension, i.e., it cannot improve the intensity of turbulent fluctuation, in the fully developed supersonic mixing layers.

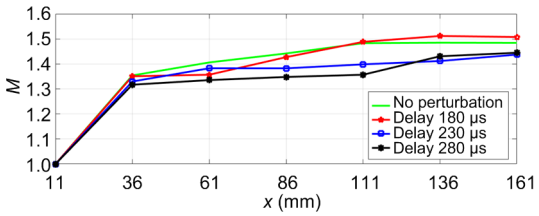

Fig. 18 Distribution of the fractal dimension of the supersonic mixing layer under different conditions

4 Conclusions

The characteristics of mixing enhancement achieved by using a pulsed PSJ were investigated via experiments. Instantaneous results were obtained by NPLS in different transverse (*Y*-*Z*), streamwise (*X*-*Z*), and spanwise (*X*-*Y*) planes. The large-scale structures induced by the pulsed PSJ actuator in the supersonic mixing layers were successfully captured by NPLS. The indexes of the fractal dimension and mixing layer thickness were measured and calculated to estimate the effect of the PSJ actuator on the supersonic mixing layers. The results obtained were as follows.

1. A PSJ can be used as an effective method for mixing enhancement based on the analysis of the NPLS results in three directions. The effects of the PSJ were remarkable in the transverse direction, and more than 8*D* in the spanwise direction.

2. The PSJ inside the large-scale vortex structures intensified the turbulent fluctuations, and the PSJ surrounding the large-scale vortex structures enlarged the scale of the vortices. The PSJ between the two large-scale vortex structures was advantageous for merging the vortices.

3. The value of the mixing layer thickness under perturbation was larger than that under no perturbation in the downstream.

4. The high-strength perturbation of the PSJ did not improve the fractal dimension values of the fully developed supersonic mixing layers.

Contributors

Peng WANG wrote the first draft of the manuscript. Chi-bing SHEN guided the design and test research work of the paper, moreover, revised and edited the final version.

Conflict of interest

Peng WANG and Chi-bing SHEN declare that they have no conflict of interest.

References

Adelgren RG, Elliott GS, Crawford JB, et al., 2005. Axisymmetric jet shear-layer excitation induced by laser energy and electric arc discharges. *AIAA Journal*, 43(4): 776-791. https://doi.org/10.2514/1.8548

Anderson KV, Knight DD, 2012. Plasma jet for flight control. *AIAA Journal*, 50(9):1855-1872. https://doi.org/10.2514/1.J051309

Benard N, Bonnet JP, Touchard G, et al., 2008. Flow control by dielectric barrier discharge actuators: jet mixing enhancement. *AIAA Journal*, 46(9):2293-2305. https://doi.org/10.2514/1.35404

Bogdanoff DW, 1983. Compressibility effects in turbulent shear layers. *AIAA Journal*, 21(6):926-927. https://doi.org/10.2514/3.60135

Chedevergne F, Léon O, Bodoc V, et al., 2015. Experimental and numerical response of a high-Reynolds-number *M*=0.6 jet to a Plasma Synthetic Jet actuator. *International Journal of Heat and Fluid Flow*, 56:1-15. https://doi.org/10.1016/j.ijheatfluidflow.2015.06.008

Collin E, Barre S, Bonnet JP, 2004. Experimental study of a supersonic jet-mixing layer interaction. *Physics of Fluids*, 16(3):765-778. https://doi.org/10.1063/1.1644574

Davis SA, Glezer A, 1999. Mixing control of fuel jets using synthetic jet technology: velocity field measurements. Proceedings of the 37th Aerospace Sciences Meeting & Exhibit. https://doi.org/10.2514/6.1999-447

Dietiker JF, Hoffmann KA, 2007. Numerical investigation of turbulent shear layers in jet exhaust flows. Proceedings of the 37th AIAA Fluid Dynamics Conference and Exhibit, p.1-25. https://doi.org/10.2514/6.2007-3856

Dimotakis PE, 1991. Turbulent free shear layer mixing and combustion. *In*: Curran ET, Murthy SNB (Eds.), High-speed Flight Propulsion Systems. American Institute of Aeronautics and Astronautics, Washington DC, USA, p.265-340. https://doi.org/10.2514/5.9781600866104.0265.0340

Falconer KJ, 2003. Fractal Geometry: Mathematical Foundations and Applications, 2nd Edition. John Wiley & Sons Ltd., Chichester, UK, p.41-57.

Feng JH, Shen CB, Wang QC, et al., 2015. Experimental and numerical study of mixing characteristics of a rectangular lobed mixer in supersonic flow. *The Aeronautical Journal*, 119(1216):701-725. https://doi.org/10.1017/S0001924000010782

Fernando EM, Menon S, 1993. Mixing enhancement in compressible mixing layers: an experimental study. *AIAA Journal*, 31(2):278-285. https://doi.org/10.2514/3.11665

Freeman AP, Catrakis HJ, 2009. Active control of mixing in turbulent separated shear layers and effects of forcing on the fractal geometry of scalar interfaces. *Journal of Turbulence*, 10:N32. https://doi.org/10.1080/14685240903338080

Gonzalez RC, Woods WR, 2010. Digital Image Processing, 3rd Edition. Ruan QQ, Ruan YZ (translators), 2011. Publishing House of Electronics Industry, Beijing, China, p.463-467.

Grossman KR, Cybyk BZ, VanWie DM, 2003. Sparkjet actuators for flow control. Proceedings of the 41st Aerospace Sciences Meeting and Exhibit, American Institute of Aeronautics and Astronautics, AIAA Paper 2003-2057. https://doi.org/10.2514/6.2003-57

Grossman KR, Cybyk BZ, Rigling MC, et al., 2004. Characterization of sparkjet actuators for flow control. Proceedings of the 42nd AIAA Aerospace Sciences Meeting and Exhibit, American Institute of Aeronautics and Astronautics, AIAA Paper 2004-2089. https://doi.org/10.2514/6.2004-89

Guirguis RH, Grinstein FF, Young TR, et al., 1987. Mixing enhancement in supersonic shear layers. Proceedings of the 25th AIAA Aerospace Sciences Meeting, American Institute of Aeronautics and Astronautics, AIAA Paper 87-0373. https://doi.org/10.2514/6.1987-373

Gutmark EJ, Schadow KC, Yu KH, 1995. Mixing enhancement in supersonic free shear flows. *Annual Review of Fluid Mechanics*, 27:375-417. https://doi.org/10.1146/annurev.fl.27.010195.002111

Haack SJ, Taylor TM, Cybyk BZ, et al., 2011. Experimental estimation of sparkjet efficiency. Proceedings of the 42nd AIAA Plasmadynamics and Lasers Conference, AIAA Paper 2011-3997.

https://doi.org/10.2514/6.2011-3997

Haimovitch Y, Gartenberg E, Roberts Jr AS, et al., 1994. An investigation of wall injectors for supersonic mixing enhancement. Proceedings of the 30th Joint Propulsion Conference and Exhibit, American Institute of Aeronautics and Astronautics, AIAA Paper 94-2940. https://doi.org/10.2514/6.1994-2940

Hardy P, Barricau P, Belinger A, et al., 2010. Plasma synthetic jet for flow control. Proceedings of the 40th Fluid Dynamics Conference and Exhibit, American Institute of Aeronautics and Astronautics, AIAA Paper 2010-5103. https://doi.org/10.2514/6.2010-5103

Huet M, 2014. On the use of plasma synthetic jets for the control of jet flow and noise. Proceedings of the 20th AIAA/CEAS Aeroacoustics Conference, American Institute of Aeronautics and Astronautics, AIAA Paper 2014-2620. https://doi.org/10.2514/6.2014-2620

Kharitonov AM, Lokotko AV, Tchernyshyev AV, et al., 2000. Mixing processes of supersonic flows in a model duct of a rocket scramjet engine. Proceedings of the 38th Aerospace Sciences Meeting and Exhibit, American Institute of Aeronautics and Astronautics, AIAA Paper 2000-0559. https://doi.org/10.2514/6.2000-559

Lazar E, Elliott G, Glumac N, 2008. Control of the shear layer above a supersonic cavity using energy deposition. *AIAA Journal*, 46(12):2987-2997. https://doi.org/10.2514/1.32835

Liao L, Yan L, Huang W, et al., 2018. Mode transition process in a typical strut-based scramjet combustor based on a parametric study. *Journal of Zhejiang University-SCIENCE A (Applied Physics & Engineering)*, 19(6): 431-451. https://doi.org/10.1631/jzus.A1700617

Lui C, Lele SK, 2001. Direct numerical simulation of spatially developing, compressible, turbulent mixing layers. Proceedings of the 39th Aerospace Sciences Meeting and Exhibit, American Institute of Aeronautics and Astronautics, AIAA Paper 2001-0291. https://doi.org/10.2514/6.2001-291

Martens S, McLaughlin DK, 1995. Mixing enhancement using Mach wave interaction in a confined supersonic shear layer. Proceedings of the Fluid Dynamics, American Institute of Aeronautics and Astronautics, AIAA Paper 95-2177. https://doi.org/10.2514/6.1995-2177

McCormick DC, Bennett Jr JC, 1994. Vortical and turbulent structure of a lobed mixer free shear layer. *AIAA Journal*, 32(9):1852-1859. https://doi.org/10.2514/3.12183

Narayanaswamy V, Shin J, Clemens NT, et al., 2008. Investigation of plasma-generated jets for supersonic flow control. Proceedings of the 46th AIAA Aerospace Sciences Meeting and Exhibit, American Institute of Aeronautics and Astronautics, AIAA Paper 2008-285. https://doi.org/10.2514/6.2008-285

Narayanaswamy V, Raja LL, Clemens NT, 2012. Control of a shock/boundary-layer interaction by using a pulsed-plasma jet actuator. *AIAA Journal*, 50(1):246-249. https://doi.org/10.2514/1.J051246

Papamoschou D, 1989. Structure of the compressible turbulent shear layer. Proceedings of the 27th Aerospace Sciences Meeting, American Institute of Aeronautics and Astronautics, AIAA-89-0126. https://doi.org/10.2514/6.1989-126

Santhanakrishnan A, Jacob JD, 2007. Flow control with plasma synthetic jet actuators. *Journal of Physics D: Applied Physics*, 40(3):637-651. https://doi.org/10.1088/0022-3727/40/3/S02

Seiner JM, Dash SM, Kenzakowski DC, 2001. Historical survey on enhanced mixing in scramjet engines. *Journal of Propulsion and Power*, 17(6):1273-1286. https://doi.org/10.2514/2.5876

Sreenivasan KR, 1991. Fractals and multifractals in fluid turbulence. *Annual Review of Fluid Mechanics*, 23: 539-604. https://doi.org/10.1146/annurev.fl.23.010191.002543

Tamburello DA, Amitay M, 2008. Active control of a free jet using a synthetic jet. *International Journal of Heat and Fluid Flow*, 29(4):967-984. https://doi.org/10.1016/j.ijheatfluidflow.2008.02.017

Wang L, Xia ZX, Luo ZB, et al., 2014a. Experimental study on the characteristics of a two-electrode plasma synthetic jet actuator. *Acta Physica Sinica*, 63(19):194702 (in Chinese). https://doi.org/10.7498/aps.63.194702

Wang L, Xia ZX, Luo ZB, et al., 2014b. Three-electrode plasma synthetic jet actuator for high-speed flow control. *AIAA Journal*, 52(4):879-882. https://doi.org/10.2514/1.J052686

Wang P, Shen C, 2019. Mixing enhancement for supersonic mixing layer by using plasma synthetic jet. *Acta Physica Sinica*, 68(17):174701 (in Chinese). https://doi.org/10.7498/aps.68.20190683

Wang QC, Wang ZG, Jing L, et al., 2013. Characteristics of mixing enhanced by streamwise vortices in supersonic flow. *Applied Physics Letters*, 103(14):144102. https://doi.org/10.1063/1.4823699

Watanabe S, Mungal MG, 2005. Velocity fields in mixing-enhanced compressible shear layers. *Journal of Fluid Mechanics*, 522:141-177. https://doi.org/10.1017/S0022112004001727

Zang A, Tempel T, Yu K, et al., 2005. Experimental characterization of cavity-augmented supersonic mixing. Proceedings of the 43rd AIAA Aerospace Sciences Meeting and Exhibit, American Institute of Aeronautics and Astronautics, AIAA Paper 2005-1423. https://doi.org/10.2514/6.2005-1423

Zhang CX, Liu Y, Fu BS, et al., 2018. Direct numerical

simulation of subsonic-supersonic mixing layer. *Acta Astronautica*, 153:50-59. https://doi.org/10.1016/j.actaastro.2018.10.004

Zhang DD, Tan JG, Lv L, 2015. Investigation on flow and mixing characteristics of supersonic mixing layer induced by forced vibration of cantilever. *Acta Astronautica*, 117:440-449. https://doi.org/10.1016/j.actaastro.2015.09.001

Zhao YX, 2008. Experimental Investigation of Spatiotemporal Structures of Supersonic Mixing Layer. PhD Thesis, National University of Defense Technology, Changsha, China (in Chinese).

Zhao YX, Yi SH, Tian LF, et al., 2008. The fractal measurement of experimental images of supersonic turbulent mixing layer. *Science in China Series G: Physics, Mechanics and Astronomy*, 51(8):1134-1143. https://doi.org/10.1007/s11433-008-0097-3

Zhou Y, Xia ZX, Luo ZB, et al., 2017. A novel ram-air plasma synthetic jet actuator for near space high-speed flow control. *Acta Astronautica*, 133:95-102. https://doi.org/10.1016/j.actaastro.2017.01.016

中文概要

题　目： 等离子体合成射流扰动在超声速流场中不同位置的截面特性以及涡结构演化

目　的： 燃料和氧化剂的快速掺混是发展超燃冲压发动机的关键技术。本文使用等离子体合成射流对超声速混合层进行增强混合，采用实验的方法获得等离子体合成射流扰动后超声速混合层的精细结构，并研究在超声速混合层中等离子体合成射流增强混合的特性。

创新点： 1. 使用纳米平面激光散射技术（NPLS）获取在超声速混合层中由等离子体合成射流诱导的大尺度涡结构；2. 分析由等离子体合成射流诱导的大尺度涡结构的演化过程。

方　法： 1. 使用信号源发生器实现纳米平面激光散射/粒子图像测速（NPLS/PIV）和脉冲电源的时序控制，从而实现 NPLS 对等离子体合成射流诱导的大尺度涡结构的捕捉，以及得到 PIV 获取流场的速度分布；2. 获得不同位置截面和不同延时时刻的流场精细结构，并分析等离子体合成射流增强混合的特性；3. 对 NPLS 结果提取湍流边界，计算湍流的混合层的厚度和分形维数。

结　论： 1. 等离子体合成射流可以对超声速混合层产生较大的扰动，展向方向扰动范围超过 8D；2. 等离子体合成射流可以增加混合层的厚度；3. 等离子体合成射流的扰动无法进一步提高充分发展的超声速混合层的分形维数。

关键词： 超声速剪切层；超声速混合层；等离子体合成射流；混合增强